

# Automatic prostate cancer detection through DCE-MRI images: all you need is a good normalization

Guillaume Lemaître<sup>a,b,\*</sup>, Robert Martí<sup>b</sup>, Fabrice Meriaudeau<sup>a,c</sup>

<sup>a</sup>*LE2I UMR6306, CNRS, Arts et Métiers, Univ. Bourgogne Franche-Comté, 12 rue de la  
Fonderie, 71200 Le Creusot, France*

<sup>b</sup>*ViCOROB, Universitat de Girona, Campus Montilivi, Edifici P4, 17071 Girona, Spain*

<sup>c</sup>*CISIR, Electrical & Electronic Engineering Department, Universiti Teknologi Petronas, 32610  
Seri Iskandar, Perak, Malaysia*

---

## Abstract

This template helps you to create a properly formatted L<sup>A</sup>T<sub>E</sub>X manuscript.

*Keywords:* DCE-MRI, prostate cancer, normalization, classification,  
quantification

---

## 1. Introduction

Prostate Cancer (PCa) is the second most frequently diagnosed men cancer,  
accounting for 899,000 cases leading to 258,100 deaths (Ferlay et al., 2010). As  
highlighted by the PI-RADS Steering Committee, the two main challenges to be  
5 addressed are (Weinreb et al., 2016): (i) the improvement of detecting clinically  
significant PCa and (ii) an increase of the confidence in benign or dormant cases,  
avoiding unnecessary invasive medical exams. In this regard, multiparametric  
Magnetic Resonance Imaging (MRI) (mpMRI) is frequently used to build robust  
Computer-Aided Detection and Diagnosis (CAD) systems to detect, localize,  
10 and grade PCa. In general, CAD systems are based on mpMRI which combines  
several of the following modalities (Lemaître et al., 2015): T<sub>2</sub> Weighted (T<sub>2</sub>-W)-  
MRI, Dynamic Contrast-Enhanced (DCE)-MRI, Apparent Diffusion Coefficient  
(ADC) maps, and Magnetic Resonance Spectroscopy Imaging (MRSI).

---

\*Corresponding author.

Email address: [g.lemaitre58@gmail.com](mailto:g.lemaitre58@gmail.com) (Guillaume Lemaître)

In DCE-MRI, a contrast media is injected intravenously and a set of images  
15 is acquired over time. Consequently, each voxel in the image is a dynamic  
signal which is related to the vascular properties of the tissue. In fact, these  
properties are automatically extracted using quantitative or semi-quantitative  
approaches (Lemaître et al., 2015).

The former group of approaches uses pharmacokinetic modelling based on a  
20 bicompartiment model, namely Brix (Brix et al., 1991) and Tofts (Tofts et al.,  
1995) models. The parameters of the Brix model are found assuming a linear  
relationship between the media concentration and MRI signal intensity. This as-  
sumption has shown, however, to lead to inaccurate parameter calculation (Heil-  
mann et al., 2006). In the contrary, Tofts model only requires a conversion from  
25 MRI signal intensity to concentration, which can become a non-linear relation-  
ship using specific equation of MRI sequences (e.g., FLASH sequence). Tofts  
modelling suffers, however, from an higher complexity (Gliozzi et al., 2011). The  
conversion using the non-linear approach requires to acquire a  $T_1$  map which  
is not always possible during clinical examination. Furthermore, the parameter  
30 calculation require the Arterial Input Function (AIF) which is challenging to  
measure and can also lead to inaccurate estimation of the parameters.

The latter group of approaches are rather mathematical than pharmacoki-  
netic modelling (Huisman et al., 2001; Gliozzi et al., 2011). These methods  
offer the advantages to not require any knowledge about the MRI sequence nor  
35 any conversion from signal intensity to concentration. However, the heuristic  
approach propose by Huisman et al. requires an estimate regarding the noise  
standard deviation of the signal as well as manual tuning.

Nevertheless, all presented methods suffer from two major drawbacks: (i)  
the inter-patient variability of the data lead to a variation of the parameters  
40 estimated and to poor classification performance while designing CAD systems,  
and (ii) only few parameters are used to characterize the dynamic signal imply-  
ing that some information are discarded.

In this work, we propose a fully automatic normalization method for DCE-  
MRI that reduce the inter-patient variability of the data. Furthermore, we show

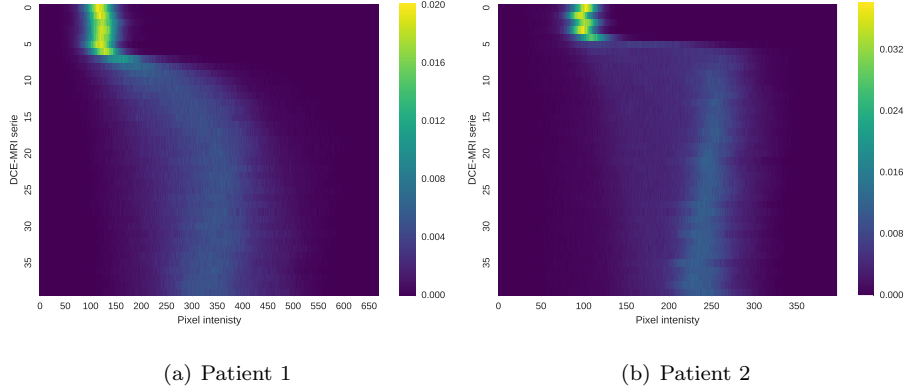


Figure 1: Illustration of the variations of the intensity PDF over time of two patients in a DCE-MRI.

that using the full normalized signal lead to the best classification performance.

The paper is organized as follows: Section 2 outlines our normalization strategy (Section 2.1) as well as specificity regarding the state-of-the-art methods used for comparison (Section 2.2). The dataset, experiments, and results are reported in Section 3 while discussed in Section 4 followed by a concluding section.

## 2. Methods

### 2.1. Normalization of DCE-MRI images

In this work, we proposed a method to normalized DCE-MRI prostate data. However, it can be note that this method can be used for any DCE-MRI sequences. The aim of the method is to reduce the intra-patient variation that can occur during the acquisition. These variations can be highlighted by observing the evolution of the intensity Probability Density Function (PDF) of the DCE-MRI over time, as shown in Fig.1. These variations are: (i) an offset of the peak value before pre-contrast, (ii) a time offset depending of the contrast injection, and (iii) a scale factor related to the enhancement. Therefore, our normalization method should attenuate all these variations

### 2.1.1. Baseline alignment of each DCE-MRI serie

Short-path using graph minimization.

### 2.1.2. Estimate the dispersion of the voxel intensities

65 MSE.

### 2.1.3. Parametric curve alignment

Model using 1 translation and one scale.

## 2.2. Quantification of DCE-MRI

### 2.2.1. Brix and Hoffmann models

70 In the Brix model (Brix et al., 1991), the MRI signal intensity is assumed to be proportional to the media concentration. Therefore, the model is expressed as in Eq. (1):

$$s_n(t) = 1 + A \left[ \frac{\exp(k_{el}t') - 1}{k_{ep}(k_{ep} - k_{el})} \exp(-k_{el}t) - \frac{\exp(k_{ep}t') - 1}{k_{el}(k_{ep} - k_{el})} \exp(-k_{ep}t) \right], \quad (1)$$

with

$$s_n(t) = \frac{s(t)}{S_0}, \quad (2)$$

where  $s(t)$  and  $S_0$  are the MRI signal intensity at time  $t$  and the average pre-contrast MRI signal intensity, respectively;  $A$ ,  $k_{el}$ , and  $k_{ep}$  are a constant proportional to the transfer constant, the diffusion rate constant, and the rate constant, respectively. Additionally, during the injection time  $0 \leq t \leq \tau$ ,  $t' = t$  and afterwards while  $t > \tau$ ,  $t' = \tau$ .

Following this model, Hoffmann et al. propose the following similar model  
80 as expressed in Eq. (3):

$$s_n(t) = 1 + \frac{A}{\tau} \left[ \frac{k_{ep}(\exp(k_{el}t') - 1)}{k_{el}(k_{ep} - k_{el})} \exp(-k_{el}t) - \frac{\exp(k_{ep}t') - 1}{(k_{ep} - k_{el})} \exp(-k_{ep}t) \right]. \quad (3)$$

The parameters are estimated by fitting the model using non-linear least-squares optimization solved with Levenberg-Marquardt.

### 2.2.2. Tofts model

The extended Tofts model is formulated as in Eq. (4):

$$C_t(t) = K_{trans}C_p(t) * \exp(-k_{ep}t) + v_pC_p(t), \quad (4)$$

85 where  $*$  is the convolution operator;  $C_t(t)$  and  $C_p(t)$  is the concentration of contrast agent in the tissue and in the plasma, respectively;  $K_{trans}$ ,  $k_{ep}$ , and  $v_p$  are the volume transfer constant, the diffusion rate constant, and the plasma volume fraction, respectively.

Therefore, Tofts model requires to: (i) detect candidate voxels from the femoral or iliac arteries and estimate a patient-based AIF signal, (ii) convert  
90 the MRI signal intensity (i.e., AIF and dynamic signal) to a concentration, and (iii) in the case of a population-based AIF, estimate an AIF signal.

#### **Segmentation of artery voxels and patient-based AIF estimation**

The AIF signal from DCE-MRI can be manually estimated by selecting the most-enhanced voxels from the femoral or iliac arteries (Meng et al., 2010).  
95 Few methods have been proposed to address the automated extraction of AIF signal. Chen et al. filter successively the possible candidates (Chen et al., 2008): (i) dynamic signals with small peak are rejecting by thresholding, (ii) voxels with a small wash-in are rejected by thresholding, (iii)  
100 a blob detector is used and large enough regions are kept, and (iv) circular and cylindricity are used to reject the last false positive. Zhu et al. propose an iterative method selecting voxels which best fit a gamma variate function (Zhu et al., 2011). However, it requires to compute first and second derivatives as well as maximum curvature points. Shanbhag et al.  
105 propose a 4-steps algorithm (Shanbhag et al., 2012; Fennessy et al., 2015): (i) remove slices with artefacts and find the best slices based on intrinsic anatomic landmarks and enhancement characteristics, (ii) find the voxel candidates using the maximum enhanced voxels and a multi-label maximum entropy based thresholding algorithm, (iii) excluding region next to the endorectal coil, and (iv) selecting the best 5 candidates which meet  
110

enhancement characteristics and that are correlated.

All the above methods are rather complex and thus we propose a method which is based on the following simple assumptions: (i) all possible AIF signal candidates should have a similar shape, (ii) an high enhancement, and (iii) the arteries should be almost round and within a size range. Therefore, each slice is clustered into regions using K-means clustering with  $k = 6$ . The cluster with the highest enhancement—i.e. corresponding to the 90<sup>th</sup> percentile of the maximum of each dynamic signal—contain the arteries and is selected. Finally, regions with an eccentricity smaller than 0.5 and an area in the range of  $[100, 400]$  voxels are kept. Additionally, to remove voxels contaminated by partial volume effect, only the 10% most enhanced voxels of the possible candidates are kept as proposed by (Schabel and Parker, 2008) and the average signal is computed. A summary of the different segmentation steps is presented in Fig. ??.

**Conversion of MRI signal intensity to concentration** To estimate the free parameters of the Tofts model (see Eq. (4)), the concentration  $C_t(t)$  and  $C_p(t)$  need to be computed from the MRI signal intensity and the AIF signal, respectively. This conversion is based on the equation of the FLASH sequence—see Appendix A for details—and is formulated as in Eq. (5):

$$c(t) = \frac{1}{TR \cdot r_1} \ln \left( \frac{1 - \cos \alpha \cdot S^* \frac{s(t)}{S_0}}{1 - S^* \frac{s(t)}{S_0}} \right) - \frac{R_{10}}{r_1}, \quad (5)$$

with,

$$S^* = \frac{1 - \exp(-TR \cdot R_{10})}{1 - \cos \alpha \cdot \exp(-TR \cdot R_{10})}, \quad (6)$$

where  $s(t)$  is the MRI signal,  $S_0$  is the MRI signal prior to the injection of the contrast media,  $\alpha$  is the flip angle,  $TR$  is the Repetition Time (TR),  $R_{10}$  is the pre-contrast tissue relaxation time also equal to  $\frac{1}{T_{10}}$ ,  $r_1$  is the relaxativity coefficient of the contrast agent.

$T_{10}$  can be estimated from the acquisition of a  $T_1$  map. However, this modality was not part of the clinical trial in this research and the value of

$T_{10}$  was fixed to 1600 ms for both blood and prostate as stated in the literature (Fennessy et al., 2015; De Bazelaire et al., 2004; Carr and Carroll, 2011).

**Estimation of population-based AIF** While estimating the pharmacokinetic parameters from Tofts model, the AIF concentration  $C_p(t)$  can be computed either from the patient or a population. We presented in the two previous sections the algorithms which allows to estimate the patient-based AIF concentration. To compare with the previous approach, we also computed a population-based AIF which will be also later used to compare the performance of both approaches. In that regard, the population-based AIF was estimated as in (Meng et al., 2010) by fitting the average patient-based AIFs to the model of Parker et al. (2006) which is formulated as in Eq. (7):

$$C_p(t) = \sum_{n=1}^2 \frac{A_n}{\sigma_n \sqrt{2\pi}} \exp\left(\frac{-(t - T_n)^2}{2\sigma_n^2}\right) + \frac{\alpha \exp(-\beta t)}{1 + \exp(-s(t - \tau))}, \quad (7)$$

where  $A_n$ ,  $T_n$ , and  $\sigma_n$  are the scaling constants, centers, and widths of the  $n^{\text{th}}$  Gaussian,  $\alpha$  and  $\beta$  are the amplitude and decay constant of the exponential; and  $s$  and  $\tau$  are the width and center of the sigmoid function, respectively.

The parameters are estimated by fitting the model using non-linear least-squares optimization solved with Levenberg-Marcquardt.

### 2.2.3. PUN model

Glozzi et al. show that Phenomenological Universalities (PUN) approach can be used for DCE-MRI analysis (Glozzi et al., 2011). The model has been successfully used in a CAD system proposed by Giannini et al. (2015). This model can be expressed as in Eq. (8):

$$s_n(t) = \exp\left[rt + \frac{1}{\beta}(a_0 - r)(\exp(\beta t) - 1)\right], \quad (8)$$

145 with

$$s_n(t) = \frac{s(t) - S_0}{S_0}, \quad (9)$$

where  $s(t)$  and  $S_0$  are the MRI signal intensity at time  $t$  and the average pre-contrast MRI signal intensity, respectively;  $r$ ,  $a_0$ , and  $\beta$  are the free parameters of the model.

The parameters are estimated by fitting the model using non-linear least-squares optimization solved with Levenberg-Marcquardt.  
150

#### 2.2.4. Semi-quantitative analysis

The semi-quantitative analysis of the DCE-MRI is equivalent to extract curve characteristics directly from the signal without a strict theoretical pharmacokinetic meaning. In this work, we use the model presented by Huisman  
155 et al. (2001) which formulate the MRI signal as in Eq. (10):

$$s(t) = \begin{cases} S_0 & 0 \leq t \leq t_0 \\ S_M - (S_M - S_0) \exp\left(\frac{-(t-t_0)}{\tau}\right) & t_0 < t \leq t_0 + 2\tau \\ S_M - (S_M - S_0) \exp\left(\frac{-(t-t_0)}{\tau}\right) + w(t - t_0 + 2\tau) & t > t_0 + 2\tau \end{cases} \quad (10)$$

where  $s(t)$  is the MRI signal intensity,  $S_0$  is the pre-contrast signal intensity,  $t_0$  is the time corresponding to the start of enhancement,  $S_M$  and  $\tau$  is the maximum of the signal and the exponential time constant, and  $w$  is the slope of the linear part.

160 Huisman et al. argue that curve fitting via least-squares minimization using Nelder-Mead algorithm leads to inaccurate estimation of the free parameters: mainly the issue come from an incorrect estimation of the start of enhancement  $t_0$  leading to incorrect estimation of the other parameters. Therefore, they propose to: (i) estimate robustly  $t_0$ , (ii) estimate  $S_0$  by averaging the samples  
165 between 0 and  $t_0$  (ii) estimate  $w$  depending if the slope is significant or not, (iii)



estimate  $S_M$  which should be the point at the intersection of the most probable slope line and the plateau.

Instead of these successive estimations, we propose a unified optimization in which  $t_0$  is fixed since that this is a key parameter. Therefore,  $t_0$  is robustly  
170 estimated from the AIF signal since that this is the most enhanced signal in which the start of enhancement is easily identifiable. The AIF signal is computed as in Section 2.2.2.  $t_0$  is estimated by finding the maximum in the beginning of the first derivative of the MRI signal. Then, the function in Eq.(10) is fitted using non-linear least squares with Trust Region Reflective algorithm.  
175 Furthermore, the parameters  $\tau$  and  $S_M$  are bounded during the optimization to ensure robust estimations.

From Eq.(10), the following features are extracted: (i) the wash-in corresponding to the slope between  $t_0$  and  $t_0 + 2\tau$ , (ii) the wash-out corresponding to the parameter  $w$ , (iii) the area under the curve between  $t_0$  and the end of the  
180 signal, (iv) the exponential time constant  $\tau$ , and (v) the relative enhancement  $S_M - S_0$ .

### 3. Experiments and results

#### 3.1. Data

The multi-parametric MRI data are acquired from a cohort of patients with  
185 higher-than-normal level of Prostate-Specific Antigen (PSA). The acquisition is performed using a 3T whole body MRI scanner (Siemens Magnetom Trio TIM, Erlangen, Germany) using sequences to obtain T<sub>2</sub>-W-MRI, DCE-MRI and Diffusion Weighted (DW)-MRI. Aside of the MRI examination, these patients also have underwent a guided-biopsy. The dataset is composed of a total of  
190 20 patients of which 18 patients have biopsy proven PCa and 2 patients are “healthy” with negative biopsies. Therefore, 13 patients have a PCa in the Peripheral Zone (PZ), 3 patients have PCa in the Central Gland (CG), 2 patients have invasive PCa in both PZ and CG and finally 2 patients are considered as “healthy”. An experienced radiologist has segmented the prostate organ — on

195 T<sub>2</sub>-W- and DCE-MRI — as well as the prostate zones (i.e., PZ and CG) and  
PCa on the T<sub>2</sub>-W-MRI.

The DCE-MRI sequence consists in a kinetic study composed of 40 samples  
over time with a time resolution of 6.5 s. These DCE-MRI sequences are resam-  
pled using the spatial information of the T<sub>2</sub>-W MRI sequence with dimensions  
200 of  $448 \times 360 \times 64$  and voxel spacing of  $0.68 \times 0.68 \times 1.25$  mm<sup>3</sup>. A linear inter-  
polation is used to compute missing data during the up-sampling. The volumes  
of the DCE-MRI dynamic are rigidly registered, to remove any patient motion  
during the acquisition. Furthermore, a non-rigid registration is performed be-  
tween the T<sub>2</sub>-W- and DCE-MRI in order to propagate the prostate zones and  
205 PCa ground-truths. The resampling is implemented in C++ using the Insight  
Segmentation and Registration Toolkit (Ibanez et al., 2005).

### 3.2. Implementation

The implementation of the registration (C++), normalization (Python), and  
classification pipeline (Python) are publicly available on GitHub<sup>1</sup>. The data  
210 used for this work are also publicly available<sup>2</sup>.

### 3.3. Results

## 4. Discussions

## 5. Conclusions and future works

## Appendix A. Conversion from FLASH signal to media concentration

215 In this appendix, we show the demonstration used to extract the agent con-  
centration from the MRI signal.

The signal equation in FLASH sequence (Haase et al., 1986) is defined as:

$$s(t) = S_{eq} \sin \alpha \cdot \frac{1 - \exp(-TR(R_{10} + r_1 c(t)))}{1 - \cos \alpha \cdot \exp(-TR(R_{10} + r_1 c(t)))}, \quad (\text{A.1})$$

---

<sup>1</sup><https://github.com/I2Cvb/lemaitre-2016-nov/tree/master>

<sup>2</sup><http://some-url.com>

Table 1: AUC of the individual features for each method.

Features	Un-normalized data		Normalized data	
	RF	NB	RF	NB
<b>Brix model</b>				
$A$	0.54	0.62	0.58	0.67
$k_{el}$	0.55	0.52	0.54	0.61
$k_{ep}$	0.51	0.52	0.51	0.58
<b>Hoffmann model</b>				
$A$	0.52	0.50	0.51	0.56
$k_{el}$	0.55	0.53	0.54	0.64
$k_{ep}$	0.55	0.50	0.53	0.66
<b>Tofts model with population AIF</b>				
$K_{trans}$	0.56	0.62	0.56	0.65
$v_e$	0.51	0.50	0.50	0.52
$v_p$	0.53	0.63	0.55	0.53
<b>Tofts model with patient AIF</b>				
$K_{trans}$	0.57	0.66	0.56	0.65
$v_e$	0.49	0.50	0.51	0.52
$v_p$	0.53	0.37	0.57	0.65
<b>PUN model</b>				
$a_0$	0.52	0.53	0.53	0.51
$r$	0.53	0.59	0.55	0.55
$\beta$	0.55	0.56	0.53	0.44
<b>Semi-quantitative analysis</b>				
wash-in	0.59	0.64	0.55	0.51
wash-out	0.52	0.50	0.56	0.66
IAUC	0.51	0.61	0.52	0.64
$\tau$	0.57	0.57	0.56	0.61
$S_M - S_0$	0.56	0.63	0.53	0.64

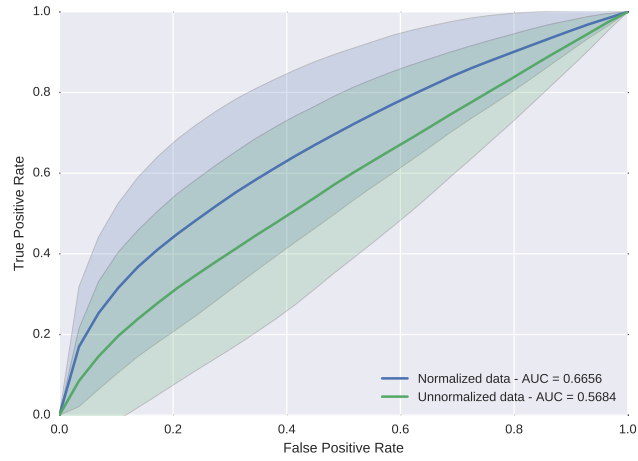


Figure 2: ROC analysis using a RF classifier using the DCE signal with and without normalization.

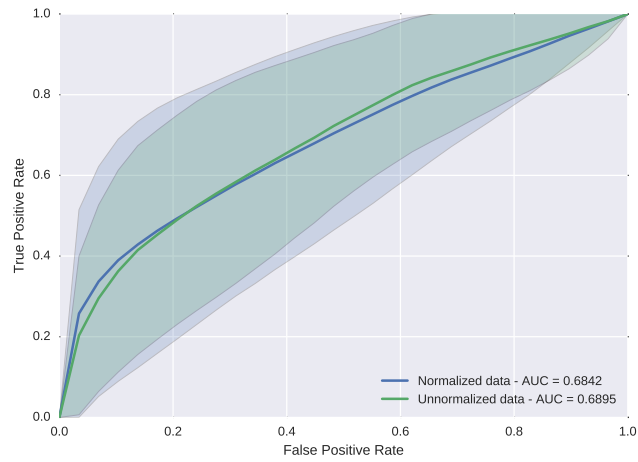


Figure 3: ROC analysis using a NB classifier using the DCE signal with and without normalization.

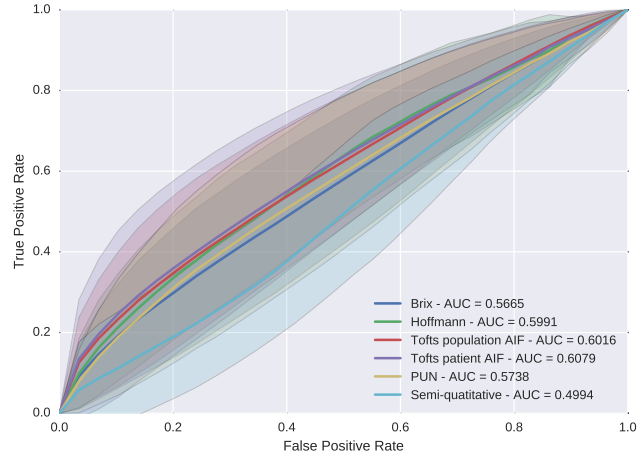


Figure 4: ROC analysis using a RF classifier for the different quantification methods without data normalization.

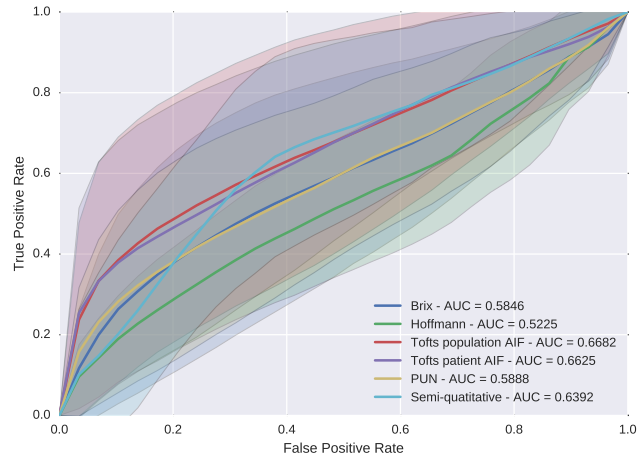


Figure 5: ROC analysis using a NB classifier for the different quantification methods without data normalization.

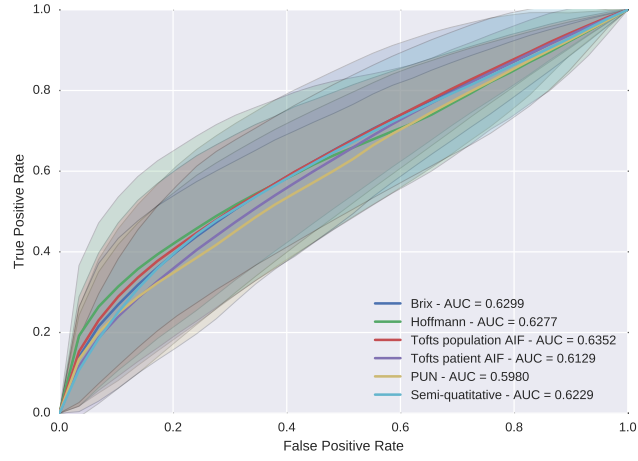


Figure 6: ROC analysis using a RF classifier for the different quantification methods with data normalization.

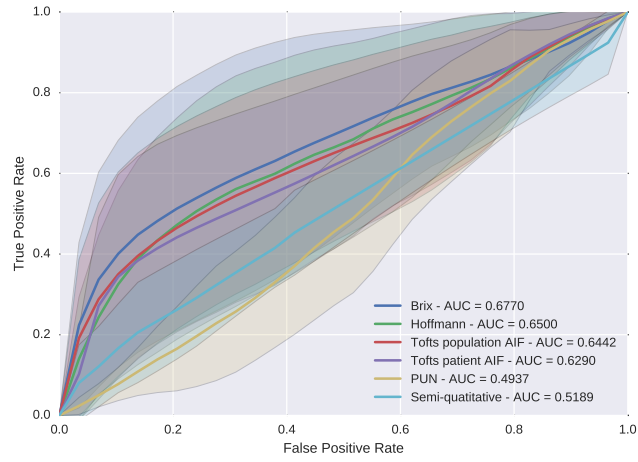


Figure 7: ROC analysis using a NB classifier for the different quantification methods with data normalization.

where  $s(t)$  is the MRI signal,  $S_{eq}$  is the maximum signal amplitude of the spoiled  
 gradient at the Echo Time (TE) which is proportional to the Proton Density  
 (PD),  $\alpha$  is the flip angle,  $TR$  is the Repetition Time (TR),  $R_{10}$  is the pre-  
 220 contrast tissue relaxation time also equal to  $\frac{1}{T_{10}}$ ,  $r_1$  is the relaxivity coefficient  
 of the contrast agent, and  $c(t)$  is the media concentration.

Therefore, the pre-contrast signal prior to bolus injection of the media is  
 defined as:

$$S_0 = S_{eq} \sin \alpha \cdot \frac{1 - \exp(-TR \cdot R_{10})}{1 - \cos \alpha \cdot \exp(-TR \cdot R_{10})}. \quad (\text{A.2})$$

225 To simplify the demonstration, let us define:

$$A = \exp(-TR \cdot R_{10}), \quad (\text{A.3})$$

$$B = \exp(-TR \cdot r_1 c(t)). \quad (\text{A.4})$$

Let us define:

$$S^* = \frac{S_0}{S_{eq} \sin \alpha}, \quad (\text{A.5})$$

$$= \frac{1 - A}{1 - A \cos \alpha}. \quad (\text{A.6})$$

Thus,

$$S^* \frac{s(t)}{S_0} = \frac{S_0}{S_{eq} \sin \alpha} \frac{s(t)}{S_0}, \quad (\text{A.7})$$

$$= \frac{1 - AB}{1 - AB \cos \alpha}. \quad (\text{A.8})$$

Now, let us define:

$$\frac{1 - \cos \alpha \cdot S^* \frac{s(t)}{S_0}}{1 - S^* \frac{s(t)}{S_0}} = \frac{1 - \cos \alpha \left( \frac{1-AB}{1-AB \cos \alpha} \right)}{1 - \frac{1-AB}{1-AB \cos \alpha}}, \quad (\text{A.9})$$

$$= \frac{1 - AB \cos \alpha - \cos \alpha (1 - AB)}{1 - AB \cos \alpha - (1 - AB)}, \quad (\text{A.10})$$

$$= \frac{1 - AB \cos \alpha - \cos \alpha + AB \cos \alpha}{1 - AB \cos \alpha - 1 + AB}, \quad (\text{A.11})$$

$$= \frac{1 - \cos \alpha}{AB(1 - \cos \alpha)}, \quad (\text{A.12})$$

$$= \frac{1}{AB}. \quad (\text{A.13})$$

Thus,

$$-TR \cdot R_{10} - TR \cdot r_1 c(t) = \ln \left( \frac{1 - \cos \alpha \cdot S^* \frac{s(t)}{S_0}}{1 - S^* \frac{s(t)}{S_0}} \right). \quad (\text{A.14})$$

230 Therefore,

$$c(t) = \frac{1}{TR \cdot r_1} \ln \left( \frac{1 - \cos \alpha \cdot S^* \frac{s(t)}{S_0}}{1 - S^* \frac{s(t)}{S_0}} \right) - \frac{R_{10}}{r_1}. \quad (\text{A.15})$$

## References

- Brix, G., Semmler, W., Port, R., Schad, L.R., Layer, G., Lorenz, W.J., 1991. Pharmacokinetic parameters in cns gd-dtpa enhanced mr imaging. *Journal of computer assisted tomography* 15, 621–628.
- 235 Carr, J.C., Carroll, T.J., 2011. *Magnetic resonance angiography: principles and applications*. Springer Science & Business Media.
- Chen, J., Yao, J., Thomasson, D., 2008. Automatic determination of arterial input function for dynamic contrast enhanced mri in tumor assessment, in: *International Conference on Medical Image Computing and Computer-Assisted Intervention*, Springer. pp. 594–601. doi:10.1007/978-3-540-85988-8\_71.
- 240 De Bazelaire, C.M., Duhamel, G.D., Rofsky, N.M., Alsop, D.C., 2004. Mr imaging relaxation times of abdominal and pelvic tissues measured in vivo at



- 3.0 t: preliminary results 1. *Radiology* 230, 652–659. doi:10.1148/radiol.2303021331.
- 245 Fennessy, F.M., Fedorov, A., Penzkofer, T., Kim, K.W., Hirsch, M.S., Vangel, M.G., Masry, P., Flood, T.A., Chang, M.C., Tempany, C.M., et al., 2015. Quantitative pharmacokinetic analysis of prostate cancer dce-mri at 3t: comparison of two arterial input functions on cancer detection with digitized whole mount histopathological validation. *Magnetic resonance imaging* 33, 886–894. doi:10.1016/j.mri.2015.02.008.
- 250 Ferlay, J., Shin, H.R., Bray, F., Forman, D., Mathers, C., Parkin, D.M., 2010. Estimates of worldwide burden of cancer in 2008: Globocan 2008. *International journal of cancer* 127, 2893–2917. doi:10.1002/ijc.25516.
- Giannini, V., Mazzetti, S., Vignati, A., Russo, F., Bollito, E., Porpiglia, F., Stasi, M., Regge, D., 2015. A fully automatic computer aided diagnosis system for peripheral zone prostate cancer detection using multi-parametric magnetic resonance imaging. *Computerized Medical Imaging and Graphics* 46, 219–226. doi:10.1016/j.compmedimag.2015.09.001.
- 255 Gliozzi, A., Mazzetti, S., Delsanto, P.P., Regge, D., Stasi, M., 2011. Phenomenological universalities: a novel tool for the analysis of dynamic contrast enhancement in magnetic resonance imaging. *Physics in medicine and biology* 56, 573.
- 260 Haase, A., Frahm, J., Matthaei, D., Hanicke, W., Merboldt, K.D., 1986. Flash imaging. rapid nmr imaging using low flip-angle pulses. *Journal of Magnetic Resonance (1969)* 67, 258–266. doi:10.1016/0022-2364(86)90433-6.
- 265 Heilmann, M., Kiessling, F., Enderlin, M., Schad, L.R., 2006. Determination of pharmacokinetic parameters in dce mri: consequence of nonlinearity between contrast agent concentration and signal intensity. *Investigative radiology* 41, 536–543. doi:10.1097/01.rli.0000209607.99200.53.

- 270 Hoffmann, U., Brix, G., Knopp, M.V., Heß, T., Lorenz, W.J., 1995. Pharmacokinetic mapping of the breast: a new method for dynamic mr mammography. *Magnetic resonance in medicine* 33, 506–514. doi:10.1002/mrm.1910330408.
- Huisman, H.J., Engelbrecht, M.R., Barentsz, J.O., 2001. Accurate estimation of  
275 pharmacokinetic contrast-enhanced dynamic mri parameters of the prostate. *Journal of Magnetic Resonance Imaging* 13, 607–614. doi:10.1002/jmri.1085.
- Ibanez, L., Schroeder, W., Ng, L., Cates, J., 2005. The itk software guide .
- Lemaître, G., Martí, R., Freixenet, J., Vilanova, J.C., Walker, P.M., Meriaudeau, F., 2015. Computer-aided detection and diagnosis for prostate cancer  
280 based on mono and multi-parametric mri: A review. *Computers in biology and medicine* 60, 8–31. doi:10.1016/j.combiomed.2015.02.009.
- Meng, R., Chang, S.D., Jones, E.C., Goldenberg, S.L., Kozlowski, P., 2010. Comparison between population average and experimentally measured arterial input function in predicting biopsy results in prostate cancer. *Academic*  
285 *radiology* 17, 520–525. doi:10.1016/j.acra.2009.11.006.
- Parker, G.J., Roberts, C., Macdonald, A., Buonaccorsi, G.A., Cheung, S., Buckley, D.L., Jackson, A., Watson, Y., Davies, K., Jayson, G.C., 2006. Experimentally-derived functional form for a population-averaged high-  
290 temporal-resolution arterial input function for dynamic contrast-enhanced mri. *Magnetic resonance in medicine* 56, 993–1000. doi:10.1002/mrm.21066.
- Schabel, M.C., Parker, D.L., 2008. Uncertainty and bias in contrast concentration measurements using spoiled gradient echo pulse sequences. *Physics in medicine and biology* 53, 2345. doi:10.1088/0031-9155/53/9/010.
- 295 Shanbhag, D., Gupta, S.N., Rajamani, K., Zhu, Y., Mullick, R., 2012. A generalized methodology for detection of vascular input function with dynamic contrast enhanced perfusion data, in: ISMRM, p. 10.

- Tofts, P.S., Berkowitz, B., Schnall, M.D., 1995. Quantitative analysis of dynamic gd-dtpa enhancement in breast tumors using a permeability model. *Magnetic Resonance in Medicine* 33, 564–568. doi:10.1002/mrm.1910330416.
- Weinreb, J.C., Barentsz, J.O., Choyke, P.L., Cornud, F., Haider, M.A., Macura, K.J., Margolis, D., Schnall, M.D., Shtern, F., Tempany, C.M., et al., 2016. Pi-rads prostate imaging-reporting and data system: 2015, version 2. *European urology* 69, 16–40.
- Zhu, Y., Chang, M.C., Gupta, S., 2011. Automated determination of arterial input function for dce-mri of the prostate, in: *SPIE Medical Imaging*, International Society for Optics and Photonics. pp. 79630W–79630W. doi:10.1117/12.878213.